Cellular/Molecular

Presynaptic Diversity Revealed by Ca^{2+}-Permeable AMPA Receptors at the Calyx of Held Synapse

Brendan Lujan, Andre Dagostin, and Henrique von Gersdorff
Vollum Institute, Oregon Health and Science University, Portland, Oregon 97239

GluA2-lacking Ca^{2+}-permeable AMPARs (CP-AMPARs) play integral roles in synaptic plasticity and can mediate excitotoxic cellular signaling at glutamatergic synapses. However, the developmental profile of functional CP-AMPARs at the auditory brainstem remains poorly understood. Through a combination of electrophysiological and live-cell Ca^{2+} imaging from mice of either sex, we show that the synaptic release of glutamate from the calyx of Held nerve terminal activates CP-AMPARs in the principal cells of the medial nucleus of the trapezoid body in the brainstem. This leads to significant Ca^{2+} influx through these receptors before the onset of hearing at postnatal day 12 (P12). Using a selective open channel blocker of CP-AMPARs, IEM-1460, we estimate that ~80% of the AMPAR population are permeable to Ca^{2+} at immature P4–P5 synapses. However, after the onset of hearing, Ca^{2+} influx through these receptors was greatly reduced. We estimate that CP-AMPARs comprise approximately 40% and 33% of the AMPAR population at P18–P22 and P30–P34, respectively. By quantifying the rate of EPSC block by IEM-1460, we found an increased heterogeneity in glutamate release probability for adult-like calyces (P30–P34). Using tetraethylammonium (TEA), a presynaptic potassium channel blocker, we show that the apparent reduction of CP-AMPARs in more mature synapses is not a consequence of presynaptic action potential (AP) speeding. Finally, through postsynaptic AP recordings, we show that inhibition of CP-AMPARs reduces spike fidelity in juvenile synapses, but not in more mature synapses. We conclude that the expression of functional CP-AMPARs declines over early postnatal development in the calyx of Held synapse.

Key words: AMPA; auditory brainstem; laser confocal Ca imaging; calyx of Held; EPSC; MNTB

Significance Statement

The calyx of Held synapse is pivotal to the circuitry that computes sound localization. Postsynaptic Ca^{2+} influx via AMPARs may be critical for signaling the maturation of this brainstem synapse. The GluA4 subunit may dominate the AMPAR complex at mature synapses because of its fast gating kinetics and large unitary conductance. The expectation is that AMPARs dominated by GluA4 subunits should be highly Ca^{2+} permeable. However, we find that Ca^{2+}-permeable AMPAR expression declines during postnatal development. Using the rate of EPSC block by IEM-1460, an open channel blocker of Ca^{2+}-permeable AMPARs, we propose a novel method to determine glutamate release probability and uncover an increased heterogeneity in release probability for more mature calyces of Held nerve terminals.

Introduction

AMPARs mediate the majority of fast excitatory transmission in the CNS. They are vital to CNS development and proper function (Traynelis et al., 2010). AMPARs are tetrameric ligand gated ion channels composed of GluA1–4 subunits that open in response to glutamate (Dingledine et al., 1999). GluA2-lacking AMPARs render the channel complex permeable to Ca^{2+} and are thus referred to as Ca^{2+}-permeable AMPARs (CP-AMPARs; Hollmann et al., 1991; Kuner et al., 2001). GluA2-containing AMPARs are impermeable to Ca^{2+} because of the single amino acid Q/R posttranscriptional editing site in the mRNA that encodes the channel pore (Burnashev et al., 1992). The majority of GluA2 subunits are edited in the brains of rodents and humans (Hume et al., 1991; Carlson et al., 2000) and animals deficient in the Q/R site editing die prematurely (Brusa et al., 1995). In several brain regions, CP-AMPARs serve important functions in the induction and modulation of activity-dependent synaptic plasticity at developing and mature synapses (Jia et al., 1996; Plant et al.,

Received Oct. 4, 2018; revised Dec. 14, 2018; accepted Jan. 3, 2019.

Author contributions: B.L. wrote the first draft of the paper; B.L., A.D., and H.v.G. edited the paper; B.L., A.D., and H.v.G. designed research; B.L. and A.D. performed research; B.L., A.D., and H.v.G. analyzed data; B.L., A.D., and H.v.G. wrote the paper.

This work was supported by the National Institute on Deafness and Other Communication Disorders–National Institutes of Health (Grants DC012938 and F32-DC017644). We thank Drs. Victor Derkach and Dale Fortin for discussions and for first suggesting the use of IEM-1460.

The authors declare no competing financial interests.

Correspondence should be addressed to Henrique von Gersdorff at vongersd@ohsu.edu.

https://doi.org/10.1523/JNEUROSCI.2565-18.2019

2006; Kim and von Gersdorff, 2016; Park et al., 2016). Additionally, Ca^{2+} permeability through this receptor regulates neuronal Ca^{2+}-induced excitotoxicity (Carriedo et al., 1998; Noh et al., 2005; Sebe et al., 2017) and the progression of several CNS pathologies are dependent on Ca^{2+} influx through these receptors (Weiss, 2011).

Mature auditory brainstem synapses possess the unique ability to maintain extremely fast and temporally precise information transmission, processes thought to be crucial for sound localization (Spirou et al., 1990; Kopp-Scheinpflug et al., 2011). Immature synapses are not immediately able to meet these demands and several synaptic specializations occur over the course of postnatal development that promote fast and indefatigable transmission (Taschenberger et al., 2002; Krächan et al., 2017). The calyx of Held nerve terminal synapses onto the principal cells in the medial nucleus of the trapezoid body (MNTB), a critical component of the ascending auditory pathway (Kandler and Friauf, 1993; Portfors and von Gersdorff, 2013). The principal cells of the MNTB undergo a developmental switch in the composition of the postsynaptic AMPARs to include GluA4 subunits; which have fast gating kinetics, large unitary conductance and rapidly recover from desensitization (Joshi et al., 2004; Koike-Tani et al., 2005). A population of AMPARs dominated by the GluA4 subunit would be expected to possess high Ca^{2+} permeability, but experiments to test the hypothesis directly have not been performed after functional maturity. Indirect measurements of the AMPAR subunit composition assayed by measuring the rectification index from EPSC IV curves recorded in the presence of intracellular polyamines suggest that these receptors should be highly permeable to Ca^{2+} because of the strong rectification. However, direct measurements of the relative levels of GluA2 subunits, the critical regulator of Ca^{2+} permeability, are not in complete agreement (Caicedo and Eybalin, 1999; Joshi et al., 2004; Koike-Tani et al., 2005). Additionally, using a CP-AMPAR specific pharmacological antagonist, <50% of the EPSC amplitude was blocked when normalized to control in experiments performed in postnatal day 14 (P14) mice (Joshi et al., 2004). This would be an unexpected result if CP-AMPAR expression remained high throughout development. Therefore, the expression profile of CP-AMPARs over the course of development requires further investigation.

Here, we examined the functional expression of CP-AMPARs over the time course of hearing onset in the mouse MNTB. Using the well characterized, CP-AMPAR-selective open-channel blocker IEM-1460 (Twomey et al., 2018), we demonstrate with patch-clamp electrophysiology and live-cell Ca^{2+} imaging that CP-AMPAR expression declines with postnatal development. This was an unexpected finding because the majority of AMPARs are GluA4 containing at mature synapses and presumed to be Ca^{2+} permeable. Additionally, we performed recordings of high-frequency action potential (AP) trains and found that the inhibition of CP-AMPARs did not affect the spiking fidelity in mature animals, whereas a strong reduction was observed in juvenile animals. We conclude that the Ca^{2+} permeability through AMPARs declines with postnatal development and suggest that most functional AMPARs must contain at least one GluR2 subunit together with GluR4 subunits at mature synapses.

Materials and Methods

Animals. All animal procedures performed in this study were approved by the Institutional Animal Care and Use Committee of Oregon Health and Science University. C57BL/6J mice (The Jackson Laboratory) of either sex were used at four postnatal day time points: P4–P5, P8–P11, P18–P22, and P27–P34. Veterinary care was provided by the Department of Comparative Medicine of Oregon Health and Science University and animals were housed in the onsite vivarium. Data were acquired from a total of 83 animals.

Electrophysiology. Brainstem slices were prepared as described previously (Lujan et al., 2016). Briefly, animals were anesthetized and killed before the brain was quickly removed and placed in an ice-cold cutting artificial CSF (ACSF). The cutting solution contained the following (in mM): 85 NaCl, 2.5 KCl, 25 glucose, 25 $NaHCO_3$, 1.25 $NaHPO_4$, 75 sucrose, 0.5 $CaCl_2$, 7 $MgCl_2$, 3 *myo*-inositol, 2 Na_2-pyruvate, and 0.4 ascorbic acid; pH 7.3 when bubbled with carbogen gas (95% O_2-5% CO_2). The meninges were removed under a dissection microscope and the brainstem was mounted on a plate for slicing with a vibratome (VT1200S; Leica Microsystems). Transverse brainstem slices containing the MNTB were made at a thickness of 200 μm and were transferred to an incubation chamber filled with normal ACSF bubbled with carbogen gas for 30–60 min at 37°C. The normal ACSF contained the following (in mM): 125 NaCl, 2.5 KCl, 25 glucose, 25 $NaHCO_3$, 1.25 $NaHPO_4$, 1.2 $CaCl_2$, 1 $MgCl_2$, 3 *myo*-inositol, 2 Na_2-pyruvate, and 0.4 ascorbic acid, osmolarity: 310–320 mOsm and pH 7.3 when bubbled with carbogen gas. Slices were maintained thereafter in normal ACSF (up to 6 h) at room temperature (23–25°C).

Brainstem slices were transferred to a recording chamber and placed under a BX51WI (Olympus) or Axioskop 2FS (Zeiss) microscope. The slices were continuously perfused at 1–2 ml/min with normal ACSF bubbled with carbogen gas. Experiments were performed at room temperature (23–25°C) unless otherwise noted. For experiments performed at more physiological temperature (PT; 33–35°C), the bath solution temperature was regulated by an inline heater and warmed platform (Warner Instruments). Neurons were visualized by infrared-differential interference contrast microscopy with a 60×/1.0 numerical aperture water-immersion objective (Olympus) connected to a CCD camera (QI-Click; QImaging). Whole-cell voltage- or current-clamp recordings were made using a HEKA EPC-10/2 amplifier controlled by Patchmaster software (HEKA). Data were acquired at 100 kHz and low-pass filtered at 2.9 kHz. Patch pipettes were pulled from standard borosilicate capillary glass (WPI) using a P97 puller (Sutter Instruments). Recording pipettes had 2.0–4.0 MΩ open-tip resistance in the bath solution. Electrophysiology data were analyzed offline using custom-written routines in IGOR Pro (WaveMetrics).

Postsynaptic voltage-clamp recordings were made from the principal cells of the MNTB using an internal solution with the following composition (in mM): 130 K-gluconate, 20 KCl, 5 Na_2 phosphocreatine, 10 HEPES, 5 EGTA, 4 Mg-ATP, 0.5 GTP, and 5 QX 314 adjusted to pH of 7.3 with KOH and osmolarity of 300–310 mOsm. To evoke EPSCs, a bipolar stimulating electrode was placed near the midline and 100 μs square pulses were applied (1–100 Hz) through an isolated stimulator (model ISO-Flex; AMPI) controlled by a Master-8 stimulator or directly through Patchmaster. To isolate the AMPAR-mediated EPSCs, we added 0.5 μM strychnine to the bath solution to inhibit glycine receptors and 10 μM bicuculline to inhibit $GABA_A$ receptors. The principal cells were held at a command voltage of −70 mV and the liquid junction potential was left uncorrected. The series resistance (R_s) was monitored throughout all experiments and online compensated electronically to 1 MΩ. Cells with uncompensated $R_s > 8$ MΩ or leak current > −200 pA were excluded from analysis. No R_s compensation was used for recording of spontaneous mEPSC events to avoid additional noise. Postsynaptic current-clamp recordings were made from the principal cells of the MNTB using the same internal solution used for voltage-clamp recordings except that QX-314 was excluded from the pipette. All current-clamp recordings were performed at PT (33–35°C) and principal cells were current injected to set the resting membrane potential to −70 mV (mean current injection = −75.3 ± 29.4 pA; $n = 14$ cells), which is close to the *in vivo* resting potential of MNTB principal cells (Lorteije et al., 2009). The compounds QX-314 and IEM-1460 were from Tocris Bioscience. OGB1 was from Invitrogen. All other reagents were purchased from Sigma-Aldrich.

Ca^{2+} imaging. To observe changes in $[Ca^{2+}]_i$, the EGTA concentration was reduced to 0.0 or 0.5 mM and the Ca^{2+} indicator Oregon Green Bapta-1 (OGB1; K_d ~170 nM) was added to the internal pipette solution

(50 μM). To ensure that the dye was maximally dialyzed into the cells, experiments were initiated 5 min after achieving whole-cell configuration. An initial voltage step was then applied to all cells and used as a control for dye loading. Synaptic activity was driven by midline stimulation and the Ca^{2+} fluorescence was recorded using an Evolve 512 EMCCD camera (Photometrics) attached to a spinning disk confocal (Yokogawa model CSU-X1) on a BX51WI microscope (Olympus) controlled by Slidebook 6 software (Intelligent Imaging Innovations). The sampling rate was 33 Hz with a 30 ms exposure time and the acquisition was TTL triggered by Patchmaster software. Fluorescence data were measured as $\Delta F/F_0$ from selected regions of interest (cell soma where AMPARs are located) using Slidebook 6 and plotted as a function of time. The EPSC responses were recorded simultaneously in voltage-clamp holding at -70 mV. Importantly, at this holding potential, NMDA receptors are nearly completely blocked and voltage-gated Ca^{2+} channels are closed (Bollmann et al., 1998).

Experimental design and statistical analysis. All data are presented as mean ± SEM. Replicate numbers (n) are presented for all experimental conditions and refer to the numbers of cells recorded per condition. Once a slice was used for an experiment, it was discarded and fresh slices were used for subsequent experiments. Statistical analysis was performed using GraphPad Prism 7.03 software for Windows. Graphs were also built in Prism and sample traces were constructed in Igor Pro. The statistical significance level was set at $p < 0.05$ and is denoted by asterisks in the figures ($*p < 0.05$, $**p < 0.005$, $***p < 0.001$); exact values are presented in the figure legends. The appropriate statistical tests were used to make comparisons between groups. A two-tailed t test was used to determine statistical significance when comparing two groups. One-way ANOVA was used to compare three groups. If a one-way ANOVA test was used, a *post hoc* multiple comparisons Tukey's test was used to compare the mean of one group with the mean of every other group. Data followed binomial distributions and parametric tests were used in all scenarios.

Results

Isolating Ca^{2+} permeable EPSCs with IEM-1460

The fast EPSCs of the MNTB principal cells are mediated by AMPARs (Forsythe and Barnes-Davies, 1993; Yang et al., 2011). To determine the contribution of CP-AMPARs to postsynaptic currents during postnatal development, we recorded EPSCs from the principal cells of the MNTB at four developmental age ranges. We chose age ranges that span the development of postnatal hearing in the mouse. During this period, the postsynaptic AMPAR subunit composition becomes specialized to ensure fast and high-fidelity transmission. EPSCs were evoked at a frequency of 1 Hz and an activity-dependent block of the EPSC was observed in the presence of IEM-1460, a selective open-channel antagonist of GluA2-lacking AMPARs (Fig. 1*A*,*B*; Sebe et al., 2017; Twomey et al., 2018). IEM-1460 blocked 78.1 ± 5.1% of the EPSC amplitude in immature P4–P5 animals, whereas a progressively smaller effect of the drug on the EPSC amplitude was observed as the age of the animals increased (P8–P11: 68.0 ± 2.6%, P18–P22: 40.8 ± 2.7%, P30–P34: 33.3 ± 5.0%; Fig. 1*C*,*D*). Importantly, the IEM-1460 block was fully reversible (Fig. 1*A*,*B*).

We also performed similar experiments in P18–P22 animals, but used the high-affinity competitive AMPAR antagonist NBQX (1 μM). Recordings in the presence of NBQX led to a rapid and near complete block of the EPSC (99.3 ± 0.1%; Fig. 1*A*). IEM-1460 and NBQX have similar molecular weights (454 Da for IEM-1460 and 380 Da for NBQX) and should reach the synaptic cleft within our brain slices at similar rates (Fig. 1*A*). We characterized the time course of the CP-AMPAR block by fitting a single exponential function to the decay of the EPSC amplitude plotted against time for all age groups (Fig. 1*A*). In P4–P5 animals, the average τ was fast: 1.4 ± 0.1 min. As the age of the animals increased, we observed a progressive slowing in the rate of CP-AMPAR block (P8–P11: 1.3 ± 0.1 min, P18–P22: 1.7 ± 0.2 min, P30–P34: 2.8 ± 0.4 min). Like MK-801, IEM-1460 is an open channel blocker and the rate of postsynaptic receptor block is partly due to presynaptic glutamate release probability (P_r), whereby synapses with high P_r will possess a relatively faster τ (Rosenmund et al., 1993). Therefore, we used the τ of postsynaptic CP-AMPAR block to estimate the relative presynaptic P_r (Fig. 1*E*). In juvenile animals, the τ was fastest and showed little variability. However, upon maturation, the average τ was slowed and displayed higher variability, which may reflect the intrinsic heterogeneity of P_r for distinct calyceal morphologies in adult-like calyces (P20–P30; Grande and Wang, 2011). This confirms previous findings of higher P_r in young synapses (P8–P10) compared with more mature (P14–P15) synapses (Taschenberger and von Gersdorff, 2000; Iwasaki and Takahashi, 2001).

The large diversity of presynaptic P_r values that we uncovered for different calyx synapses at P30–P34 may reflect differences in active zone proteins, Ca^{2+} channel expression, and the superpriming of a subset of docked vesicles (Chen et al., 2015; Taschenberger et al., 2016). Differences in the spontaneous and sound-evoked spike activity among *in vivo* calyx synapses during postnatal development may drive these changes in P_r, as well as changes in presynaptic calyx morphology and AMPAR expression (Tokuoka and Goda, 2008; Ford et al., 2009).

These results suggest that CP-AMPAR-mediated synaptic transmission declines during postnatal development at the principal cells of the MNTB. Although CP-AMPAR-mediated transmission continued to decline up to P30–P34, the largest difference observed over the developmental windows that we assayed was between the P8–P11 (prehearing) and P18–P22 (posthearing) groups. Therefore, our subsequent experiments focused on these age ranges.

To further investigate the possibility that CP-AMPAR mediated synaptic transmission declines with synapse maturation, we investigated whether spontaneous miniature EPSC (mEPSC) amplitudes were antagonized to a similar extent as the evoked EPSCs (eEPSCs) by IEM-1460 across development. Therefore, we recorded mEPSCs in control conditions and after blocking CP-AMPARS with the 1 Hz stimulation protocol in the presence of IEM-1460 (Fig. 2*A*). The mEPSC amplitude was reduced by 34.9 ± 3.7% in the P18–P22 group, similar to the effect of IEM-1460 on the eEPSC (40.8 ± 2.7%). However, mEPSC peak amplitude was only reduced by 42.9 ± 2.3% in the P8–P11 group, in contrast to the eEPSC reduction (68.0 ± 2.6%; Fig. 2*B*). We observed no change in the frequency of events with IEM-1460 in the P8–P11 group or in the P18–P22 group, suggesting no direct presynaptic effects of IEM-1460 (Fig. 2*C*). We then compared the percentage block induced by IEM-1460 on the mEPSC amplitudes at the two developmental time points and found that it was not different between the two groups (Fig. 2*D*). To further investigate the discrepancy observed between the percentage block of IEM-1460 on the mEPSCs and eEPSCs in the P8–P11 group, we constructed histograms of the mEPSC peak amplitudes. The control amplitude distributions (P8–P11 and P18–P22) were well fit with a Gaussian function ($R^2 = 0.9250$ and $R^2 = 0.9548$, respectively; Fig. 2*E*,*F*). Addition of IEM-1460 to the slices produced a leftward shift to the distributions at both ages. For the IEM-1460 distribution curve fits, we constrained the mean value to that predicted if the mEPSCs were antagonized proportionally to the eEPSCs (P8–P11: mean was set to 21.5 pA; P18–P22: mean was set to 44.2 pA). Constraining the mean of the curve fits closely approximated our data, especially in the P18–P22 group ($R^2 = 0.9500$). However in the P8–P11 group, treatment with IEM-1460 shifted the distribution such that the fit invaded the

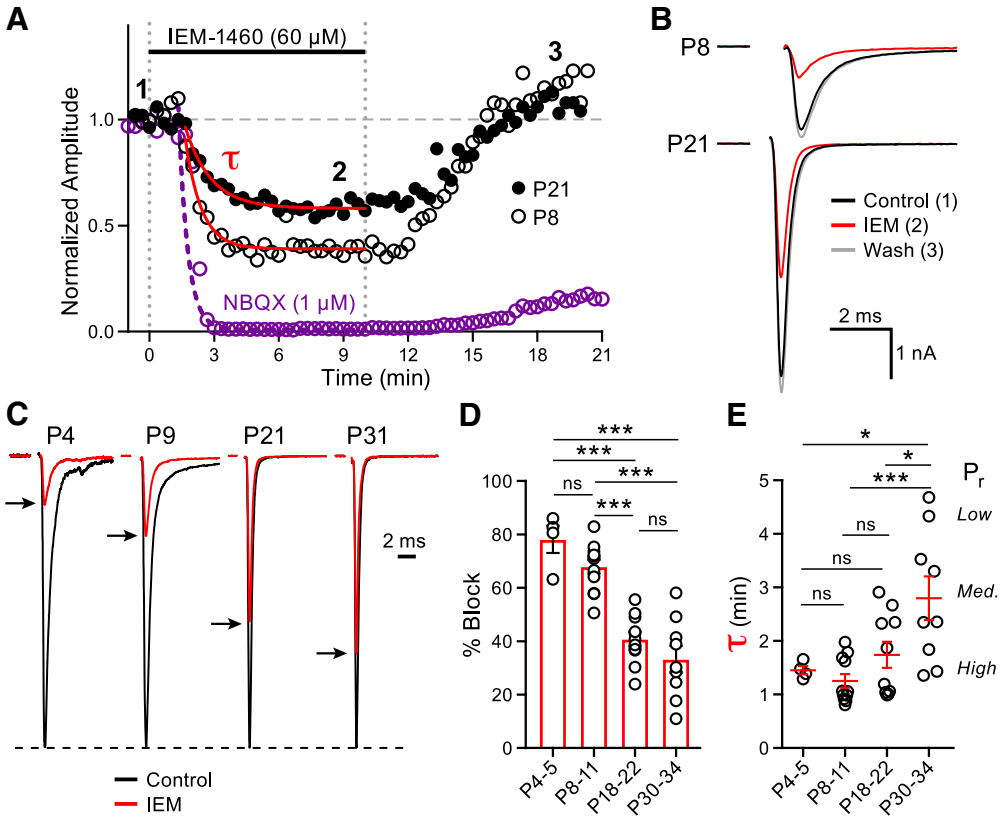

Figure 1. Release probability and CP-AMPAR mediated synaptic transmission declines during MNTB principal cell maturation. ***A***, Normalized EPSC peak amplitudes evoked at 1 Hz (downsampled to 0.05 Hz) plotted against time in representative recordings from P8 and P21 animals (open and closed black circles, respectively). EPSC amplitudes are shown in control conditions (time point 1), after the addition of IEM-1460 (60 μM; time point 2), and during washout (time point 3). External Ca^{2+} is 1.2 mM. The average normalized EPSC response recorded from P18–P22 animals ($n = 6$) in the presence of NBQX (1 μM, purple) is shown for comparison. τ of the EPSC block was fit by a single exponential function for IEM-1460 (P8: $\tau = 0.81$ min; P21: $\tau = 1.20$ min) and NBQX (P18–P22: $\tau = 0.43$ min). ***B***, Average from 20 EPSCs of the P8 (top) and P21 (bottom) animals at each designated time point in ***A*** displayed with the stimulus artifacts blanked for clarity. ***C***, Representative normalized EPSC amplitudes from P4, P9, P21, and P31 animals in control (black traces) and in the presence of IEM-1460 (red traces with peaks indicated by black arrows). ***D***, Summary data of the percentage block induced by application of IEM-1460 at the four developmental age ranges (one-way ANOVA with *post hoc* Tukey's test; P4–P5: $n = 4$, P8–P11: $n = 12$, P18–P22: $n = 11$, P30–P34: $n = 9$; P4–P5 vs P8–P11: $p = 0.39$, P4–P5 vs P18–P22: $p < 0.0001$, P4–P5 vs P30–P34: $p < 0.0001$, P8–P11 vs P18–P22: $p < 0.0001$, P8–P11 vs P30–P34: $p < 0.0001$, P18–P22 vs P30–P34: $p = 0.44$). ***E***, Summary data of the τ is shown for the four age groups (one-way ANOVA with *post hoc* Tukey's test; P4–P5 vs P8–P11: $p = 0.97$, P4–P5 vs P18–P22: $p = 0.93$, P4–P5 vs P30–P34: $p = 0.042$, P8–P11 vs P18–P22: $p = 0.51$, P8–P11 vs P30–P34: $p = 0.009$, P18–P22 vs P30–P34: $p = 0.035$). τ reflects a weighted mean of low and high vesicle fusion probabilities at different active zones and was used as a measure of relative P_r. In the P4–P5 age range, we observed uniformly high P_r values, whereas the adult-like P30–P34 age range has a diversity of P_r values from high to low. ns, nonsignificant, *$p < 0.05$, ***$p < 0.001$.

distribution of electrical noise ($R^2 = 0.6544$). This result suggests that a population of the mEPSCs with small amplitude were being masked by the electrical noise in the presence of IEM-1460 in the P8–P11 group. From these data, we conclude that the mEPSCs are probably similarly antagonized as the eEPSCs across development and that the discrepancy of percentage block observed between mEPSCs and eEPSCs in the P8–P11 group is likely due to an under sampling of events with very small amplitude. These data again suggest that postsynaptic CP-AMPAR mediated synaptic transmission declines with postnatal development.

The frequency of control mEPSC events increased ~10-fold from P8–P11 to P18–P22 (Fig. 2*A*,*C*), suggesting a larger number of functional active zones at P18–P22 synapses (Taschenberger et al., 2002). Release probability of spontaneous vesicle fusion thus appears to increase with age, whereas the P_r of action-potential-evoked vesicle fusion decreases with age (Kavalali, 2015).

High-frequency EPSC trains in IEM-1460

We next investigated whether CP-AMPARs could regulate the short-term plasticity (STP) at the developing calyx of Held synapse (von Gersdorff and Borst, 2002). We recorded EPSCs elicited by high-frequency stimulation (HFS) trains evoked at 100 Hz in P8–P11 and P18–P22 animals in control conditions and after repetitive stimulation in the presence of IEM-1460 (Fig. 3*A*). To compare the activity-dependent effect of CP-AMPAR block on STP, we constructed peak amplitude surface plots (Fig. 3*B*). The EPSC peak amplitude is displayed as a function of stimulus number with an additional *z*-axis representing the sweeps recorded sequentially. The control condition is portrayed as sweep 1 on the *z*-axis and each subsequent sweep was recorded in the presence of IEM-1460. We found that neither the paired-pulse ratio nor the τ was affected after blocking the CP-AMPARs (Fig. 3*C*,*D*). The EPSCs were inhibited more strongly in the P8–P11 group (57.6 ± 8.2%) than in the P18–P22 group (36.0 ± 13.4%) after repetitive HFS in the presence of IEM-1460, as evidenced in the surface plot (Fig. 3*B*,*E*,*F*). We compared the HFS first EPSC percentage block to that obtained using the 1 Hz stimulation protocol in Figure 1*D* to test whether the HFS train protocol equally blocked CP-AMPARs. We found that the 1 Hz stimulation and HFS protocols equally antagonized CP-AMPARs (Fig. 3*F*). From these experiments, we conclude that CP-AMPARs do not regulate the STP and that HFS in the presence of IEM-1460 does not further an-

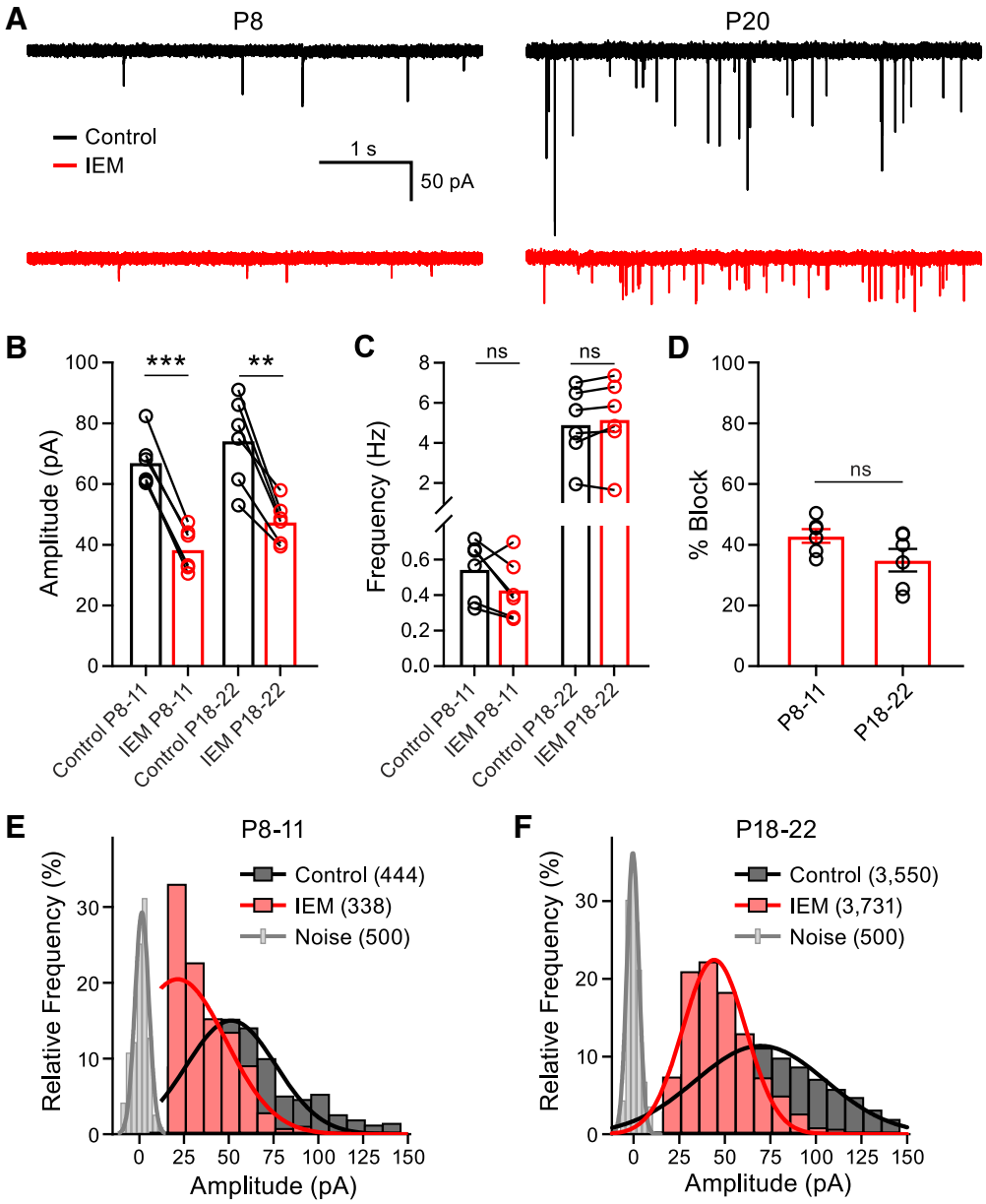

Figure 2. Blocking CP-AMPARs suppresses spontaneous mEPSC amplitudes. ***A***, Representative mEPSCs recorded at a holding potential of −70 mV from a P8 (left) and a P20 (right) animal in control conditions (black) and after the addition of IEM-1460 (red). ***B***, mEPSC peak amplitude is reduced in P8–P11 and P18–P22 animals after the addition of IEM-1460 (paired *t* test; P8–P11: $n = 6, p < 0.0001$; P18–P22: $n = 6, p = 0.0019$). ***C***, Frequency of the mEPSCs was not altered by IEM-1460 (paired *t* test; P8–P11: $n = 6, p = 0.1173$; P18–P22: $n = 6, p = 0.1494$). ***D***, Percentage block induced by IEM-1460 between the P8–P11 and P18–P22 groups was not different (unpaired *t* test; P8–P11: $n = 6$; P18–P22: $n = 6$; $p = 0.0955$). ***E***, ***F***, Frequency distribution of mEPSC peak amplitudes (bin size = 10 pA) for the P8–P11 and P18–P22 groups, respectively, in control conditions (black) or after the addition of IEM-1460 (red). The distribution of electrical noise is shown in gray. The total numbers of events per condition are shown in parentheses in the figure. ns, nonsignificant, $^{**}p < 0.005$, $^{***}p < 0.001$.

tagonize the EPSCs compared with the 1 Hz stimulation protocol, although HFS releases more glutamate overall.

Synaptically evoked Ca^{2+} transients in the principal cells of the MNTB

Our EPSC data suggested that CP-AMPAR mediated transmission declined upon synaptic maturation. We sought to confirm this finding using Ca^{2+} imaging as an alternative approach. In an effort to measure synaptically evoked CP-AMPAR-mediated Ca^{2+} transients in the MNTB principal cells, we performed whole-cell recordings and included the Ca^{2+} indicator OGB1 in the recording pipette. First, a short voltage-clamp step depolarization to −10 mV (>5 min after break-in) was applied to all cells and used as a dye-loading control. This depolarizing pulse produced a robust Ca^{2+} signal compared with quiescent (baseline) conditions (Fig. 4*A*). The principal cells were subsequently voltage clamped at −70 mV. When applying midline afferent fiber stimulation at a frequency of 100 Hz for 500 ms, we detected a 5.5 ± 0.7% increase in fluorescence in the P8–P11 group. Application of IEM-1460 to the slices blocked 54.2 ± 5.3% of this response, resulting in a 2.5 ± 0.3% increase in fluorescence (Fig. 4*B1–B3*). These data suggest that the Ca^{2+} signal detected was primarily due to Ca^{2+} influx through CP-AMPARs. When we performed similar experiments in the P18–P22 group, the synaptically evoked Ca^{2+} transients were greatly reduced (2.7 ±

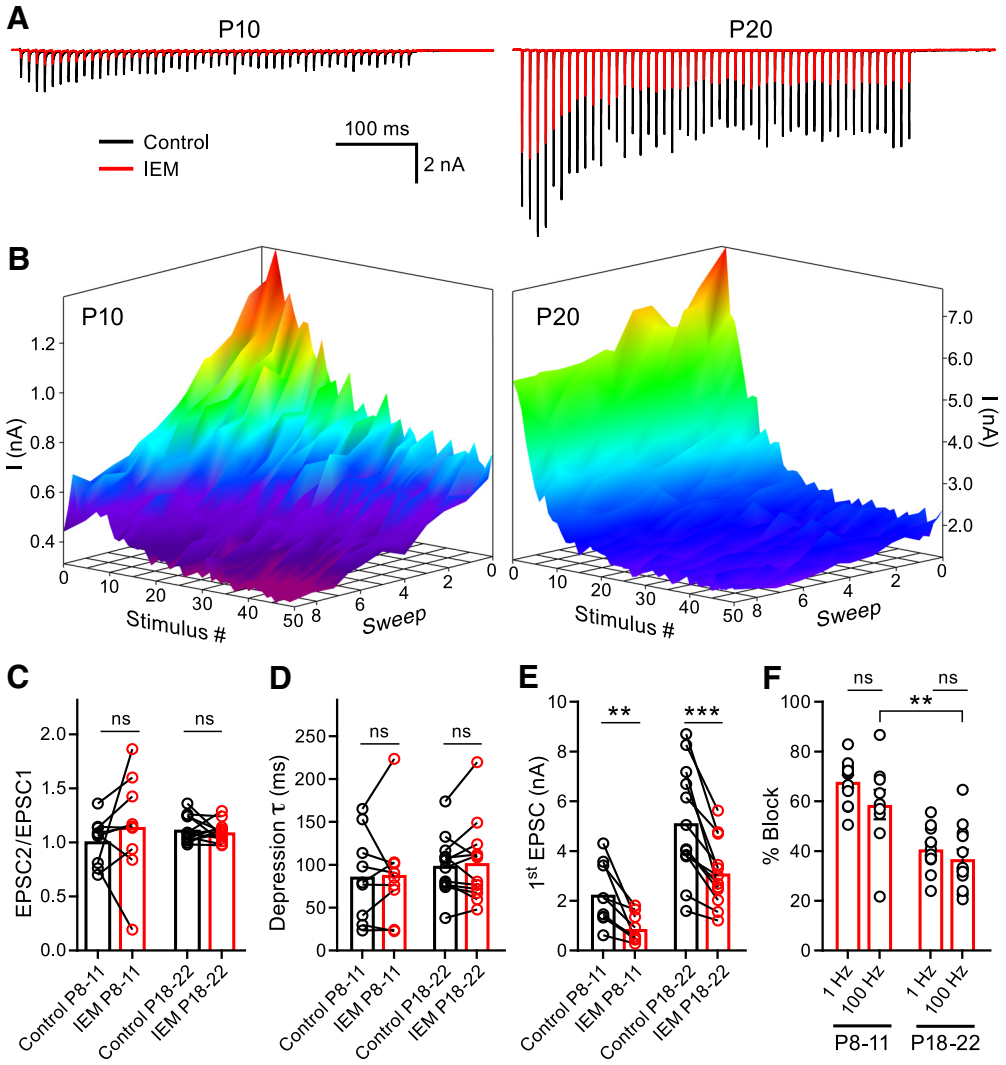

Figure 3. CP-AMPARs do not regulate STP. ***A***, EPSC trains evoked by midline stimulation at a frequency of 100 Hz were recorded in control conditions (black) and after application of IEM-1460 (red). Representative traces are displayed for a P10 (left) and a P20 (right) animal. External Ca^{2+} is 1.2 mM. ***B***, Ten sweeps (*z*-axis) of stimulation at 100 Hz (50 stimuli - *x*-axis) every 10 s yield EPSCs with peak amplitudes (*y*-axis) displayed as surface plots for representative P10 and P20 recordings. The control condition (shown as sweep 1) was an average of ≥3 trains. The surfaces are pseudo-colored depicting red for greater amplitudes and purple for smaller. Note the greater block by IEM-1460 in each successive sweep compared with the control at P10, but not at P20. ***C***, ***D***, Summary of paired-pulse ratio (paired *t* test; P8–P11: $n = 9, p = 0.2554$; P18–P22: $n = 12, p = 0.4875$) and τ (paired *t* test; P8–P11: $n = 9, p = 0.9521$; P18–P22: $n = 12, p = 0.8049$) before and after application of IEM-1460. ***E***, Summary data of the first EPSC amplitude block by IEM-1460 (paired *t* test P8–P11: $n = 9, p = 0.0036$; P18–P22: $n = 12, p = 0.0003$). ***F***, First EPSC percentage block is stronger in the P8–P11 group than in the P18–P22 group using the 100 Hz blocking protocol (unpaired *t* test; P8–P11: $n = 9$; P18–P22: $n = 12$; $p = 0.0044$). Additionally, the effect of IEM-1460 on EPSC percentage block is similar using either the 1 Hz (from Fig. 1*D*) or 100 Hz stimulation paradigms in both age groups (unpaired *t* test P8–P11: $p = 0.1339$; P18–P22: $p = 0.4171$). ns, nonsignificant, $^{**}p < 0.005$, $^{***}p < 0.001$.

0.6% increase in fluorescence). The addition of IEM-1460 had no further effect on this response (IEM-1460: 2.8 ± 0.6% increase in fluorescence; Fig. 4*C1–C3*). These data suggest that CP-AMPAR-mediated synaptic transmission declines during synaptic maturation.

However, the results of these experiments left us with two major unresolved questions: (1) what process contributed to the remaining unblocked Ca^{2+} response in the P8–P11 group? and (2) why was there no apparent contribution of CP-AMPARs to the Ca^{2+} response in the P18–P22 group, although we estimated ~40% of the AMPAR population were CP-AMPARs by means of electrophysiology? We first tested whether the remaining component of the Ca^{2+} transient in the P8–P11 group was mediated by acid-sensing ion channels (ASICs), which have recently been shown to mediate a component of the synaptically evoked postsynaptic current and Ca^{2+} transient in the MNTB (González-Inchauspe et al., 2017). We tested the contribution of ASICs with the pore blocker amiloride (Waldmann et al., 1997). We recorded EPSC trains while simultaneously imaging Ca^{2+} transients with OGB-1 in P8–P11 animals (Fig. 5*A1*,*A2*). We found that IEM-1460 inhibited the first EPSC and that subsequent application of IEM-1460 + amiloride (750 μM) further reduced the first EPSC amplitude by 28.5 ± 3.3% without affecting STP (Fig. 5*B–D*). These data confirm that ASIC-mediated currents contribute to the EPSC (González-Inchauspe et al., 2017). The Ca^{2+} imaging similarly yielded Ca^{2+} transients that could be inhibited by IEM-1460 and, after the addition of IEM-1460 + amiloride, we found a further 18.1 ± 6.2% block of the Ca^{2+} signal compared with IEM-1460 alone (Fig. 5*E1–E3*). We thus conclude that Ca^{2+} transients elicited by afferent fiber stimulation in the immature MNTB principal cells enter via two distinct routes: one route is through CP-AMPARs and the other is through ASICs gated by proton release.

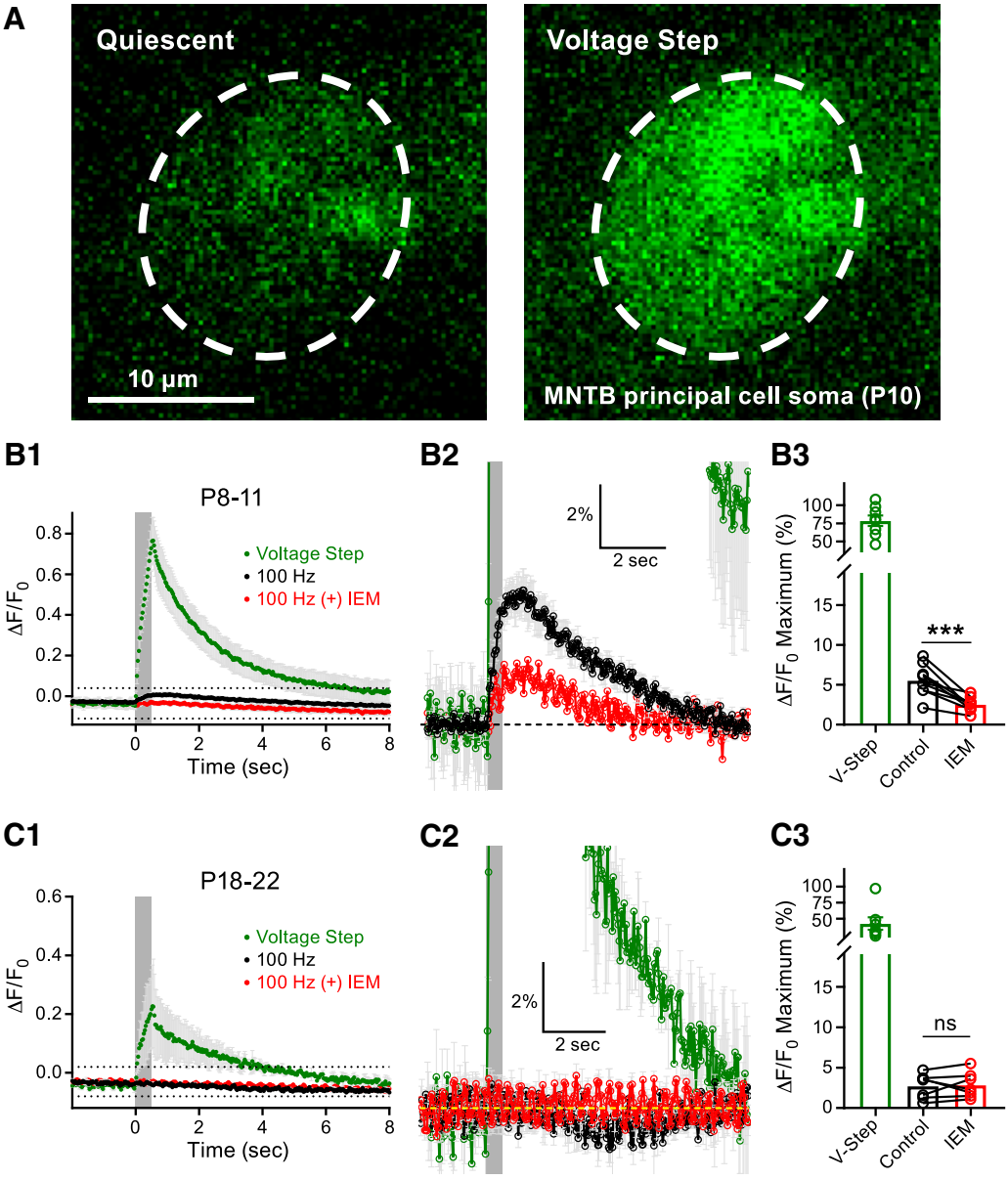

Figure 4. CP-AMPAR-mediated Ca^{2+} transients in the MNTB principal cells are developmentally regulated. ***A***, Representative MNTB principal cell loaded with the Ca^{2+} indicator OGB1 (50 μM) at >5 min after break-in at a holding potential of −70 mV during quiescent conditions (left) or during a short postsynaptic voltage depolarization to −10 mV (right). Scale bar, 10 μm. ***B1***, CP-AMPAR mediated Ca^{2+} transients induced by afferent fiber stimulation at a frequency of 100 Hz for 500 ms (gray box denotes stimulation) in P8–P11 animals during control conditions (black) or after application of IEM-1460 (red). The Ca^{2+} response observed during the voltage-step (green) is included for comparison. The region outlined by dotted lines is shown at higher magnification in ***B2***. ***B3***, Summary data of the peak Ca^{2+} responses in the P8–P11 group (paired *t* test; $n = 9$, $p = 0.0008$). ***C1***, Ca^{2+} transients recorded as in ***B1*** but in P18–P22 animals. The region outlined by dotted lines is shown at higher magnification in ***C2***. ***C3***, Summary data of the peak Ca^{2+} responses in the P18–P22 group (paired *t* test; $n = 7$; $p = 0.79$). ns, nonsignificant, ***$p < 0.001$.

Broadening mature presynaptic APs with TEA

To address our second unresolved question as to why there was an undetectable contribution of CP-AMPARs to the synaptically evoked Ca^{2+} transients in the P18–P22 group, we focused on the presynaptic AP waveform. During postnatal development, the presynaptic AP width becomes briefer at the calyx of Held synapse, which underpins the progressively lower P_r (Taschenberger and von Gersdorff, 2000). To control for the possibility that presynaptic AP speeding was the underlying cause of the apparent decrement in the number of CP-AMPARs after the onset of hearing, we pharmacologically manipulated the mature presynaptic AP shape in P18–P22 animals to a waveform that more closely resembled that of P8–P11 animals. We used TEA to block potassium channels and induce spike broadening and thus permit the entry of more Ca^{2+} ions to the presynaptic nerve terminal (Wang and Kaczmarek, 1998; Johnston et al., 2010). We recorded HFS EPSC trains in control conditions or in the presence of TEA (100 μM; Fig. 6*A*). We observed an initial facilitation and mild depression of the control EPSC train for P18–P22 in more physiological 1.2 mM external Ca^{2+} (Hermann et al., 2007; Lorteije et al., 2009) and found that the first EPSC was potentiated and that the paired-pulse ratio was decreased by the application of TEA (Fig. 6*B*,*C*). Using the Elmqvist and Quastel method to estimate readily releasable vesicle pool (RRP) size and P_r, a method reliant on the initial responses of a stimulus train (Taschenberger et al., 2002), we found that TEA increases presynaptic P_r, leaving the size of the RRP un-

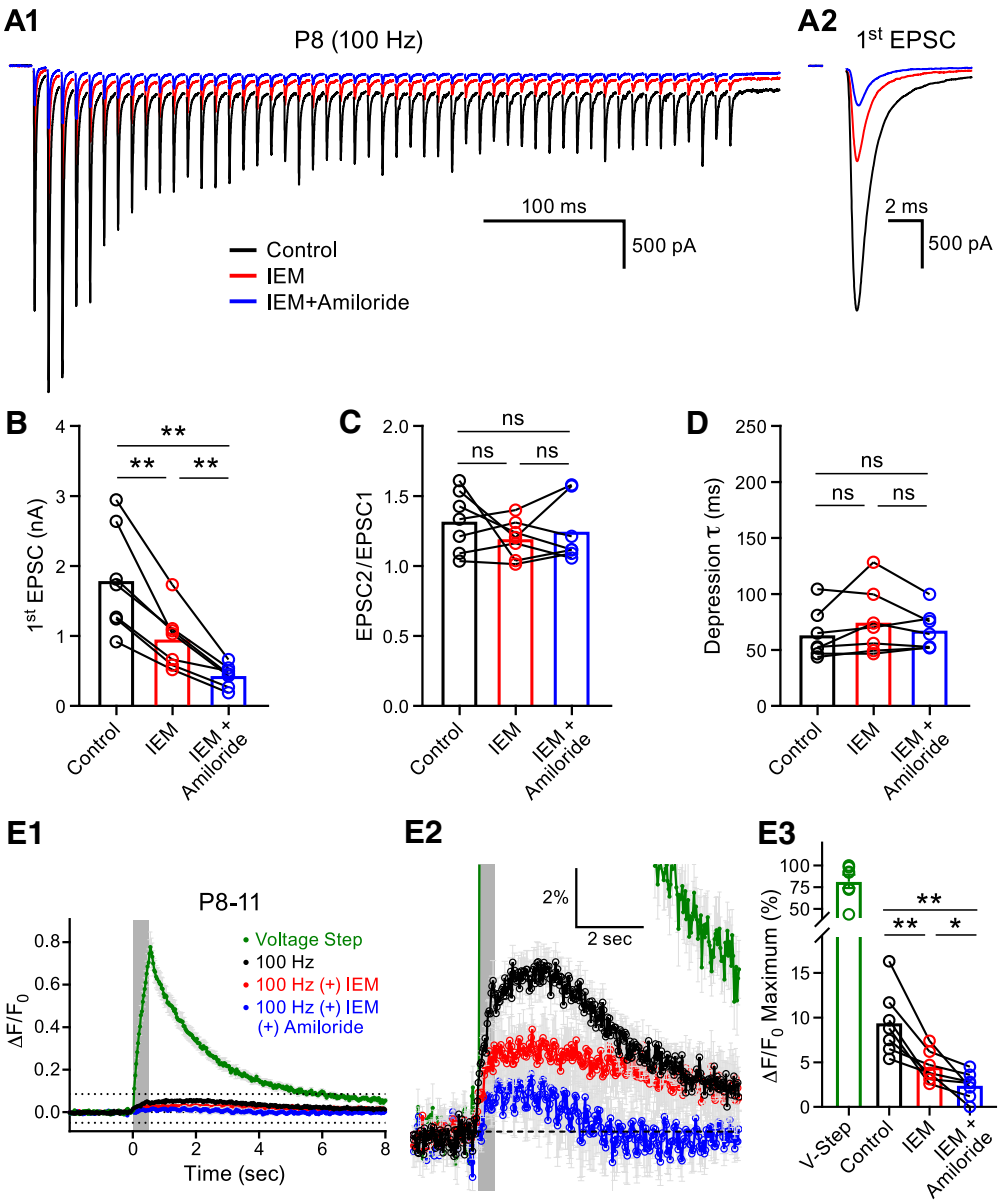

Figure 5. ASIC-mediated synaptic currents and Ca^{2+} transients in the juvenile MNTB Principal cell. ***A1***, Representative EPSC traces (100 Hz for 500 ms, left) evoked by midline stimulation are displayed from a P8 animal in control conditions (black), after the addition of IEM-1460 (red, 60 μM), and after the addition of IEM-1460 (60 μM) + amiloride (blue, 750 μM). The first EPSC from the train is enlarged in ***A2*** for comparison and the summary data for their amplitude is shown in ***B*** (one-way ANOVA with *post hoc* Tukey's test; $n = 7$; control vs IEM-1460: $p = 0.0046$, control vs IEM-1460 + amiloride: $p = 0.0034$, IEM-1460 vs IEM-1460 + amiloride: $p = 0.0081$). ***C***, ***D***, Neither IEM-1460 nor IEM-1460 + amiloride application altered the STP parameters of paired-pulse ratio (***C***: $n = 7$, one-way ANOVA with *post hoc* Tukey's test, control vs IEM-1460: $p = 0.4352$, control vs IEM-1460 + amiloride: $p = 0.7354$, IEM-1460 vs IEM-1460 + amiloride: $p = 0.7217$) or τ (***D***: control vs IEM-1460: $p = 0.2928$, control vs IEM-1460 + amiloride: 0.7719, IEM-1460 vs IEM-1460 + amiloride: $p = 0.4437$). ***E1***, Ca^{2+} transients in the postsynaptic MNTB principal cells were measured using OGB1 evoked by afferent fiber stimulation at a frequency of 100 Hz for 500 ms (gray box denotes stimulation) in control conditions (black), after the addition of IEM-1460 (red), and after the addition of IEM-1460 + amiloride (blue). The green trace represents the Ca^{2+} transient from a voltage step. The region outlined by dotted lines in ***E1*** is shown at higher magnification in ***E2***. Application of IEM-1460 + amiloride further reduced the MNTB principal cell Ca^{2+} transient compared with IEM-1460 alone. ***E3***, Summary data of the peak Ca^{2+} responses in the P8–P11 group (one-way ANOVA with *post hoc* Tukey's test, $n = 7$; control vs IEM-1460: $p = 0.0068$, control vs IEM-1460 + amiloride: $p = 0.0068$, IEM-1460 vs IEM-1460 + amiloride: $p = 0.0445$). ns, nonsignificant, $^*p < 0.05$, $^{**}p < 0.005$.

changed (Elmqvist and Quastel, 1965; Neher, 2015; Fig. 6*D1–D3*). We observed a high heterogeneity of P_r (range 0.05–0.25) and RRP size at these P18–P22 calyx synapses, which may reflect distinct calyceal morphologies and the diverse Ca^{2+} influx at stalks and swellings (Grande and Wang, 2011; Spirou et al., 2008; cf.Figs. 1*E*, 6*D3*).

We next investigated whether IEM-1460 application similarly antagonized the CP-AMPARs of P18–P22 synapses in the continued presence of TEA as in control conditions. We recorded HFS EPSC trains and blocked CP-AMPARs with IEM-1460 (Fig. 7*A*). We found that the addition of IEM-1460 to slices in the continued presence of TEA reduced the amplitude of the first EPSC (Fig. 7*B*) and produced an equal percentage block of the first EPSC compared with those experiments performed in the presence of IEM-1460 alone (Fig. 7*C*). These data confirm that the apparent reduction in CP-AMPARs present in mature P18–P22 animals is not an artifact of presynaptic AP speeding. Additionally, these data confirm that our IEM-1460-blocking protocol in the absence of TEA saturated CP-AMPAR block because increasing presynaptic gluta-

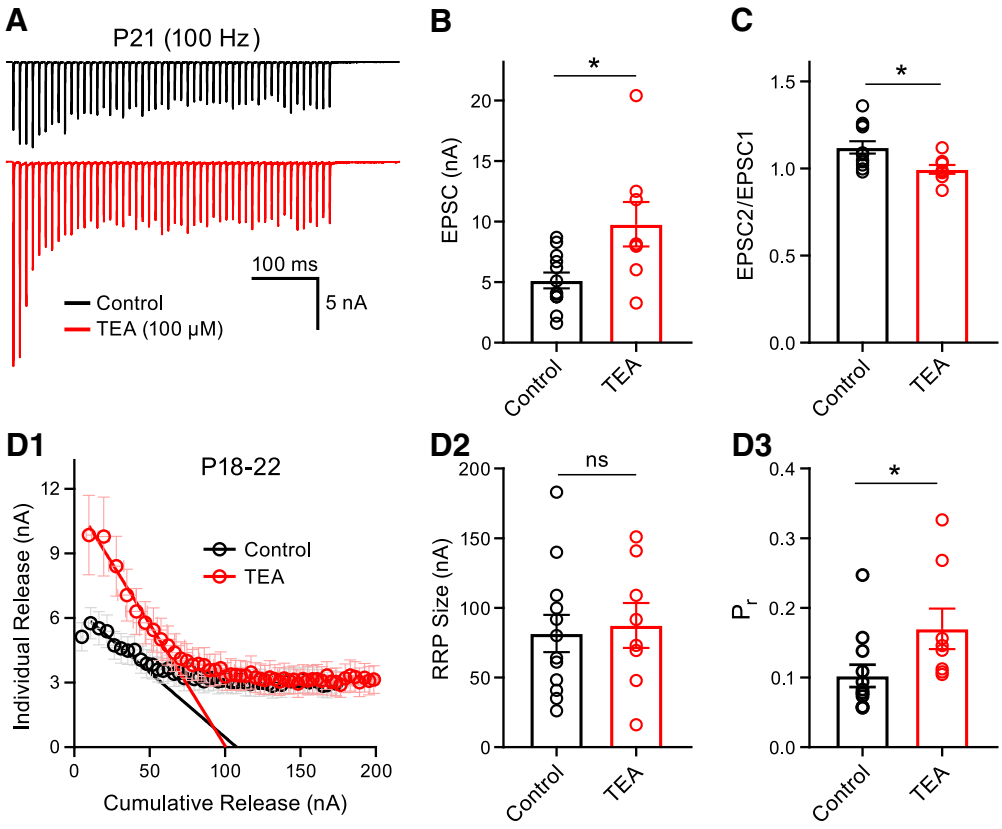

Figure 6. TEA-induced presynaptic spike broadening potentiates synaptic vesicle release. ***A***, EPSCs were evoked by midline stimulation in a P21 animal at a frequency of 100 Hz for 500 ms and the peak amplitude is plotted as a function of time in control conditions (black) or in the presence of TEA (red, 100 μM). Cell-matched recordings were not performed for every data point. ***B***, Summary data for the first EPSC amplitude is displayed and the EPSCs were potentiated in the presence of TEA (unpaired *t* test; control: $n = 12$; TEA: $n = 8$, $p = 0.0134$). ***C***, Paired-pulse ratio was reduced (unpaired *t* test; control: $n = 12$; TEA: $n = 8$, $p = 0.0186$). ***D1***, The Elmqvist and Quastel method was used to estimate presynaptic P_r and RRP size. The individual release (EPSC amplitudes during the stimulus train) was plotted as a function of the cumulative release (sum of EPSCs) in control (black) or in TEA (red). ***D2***, Size of the RRP was unchanged in TEA (unpaired *t* test; control: $n = 12$; TEA: $n = 8$, $p = 0.7858$). ***D3***, Presynaptic P_r was increased in the presence of TEA (unpaired *t* test; control: $n = 12$; TEA: $n = 8$, $p = 0.0406$). Note that control synapses display a high heterogeneity of RRP size and a diverse range of P_r values from 0.05 to 0.25 for P18–P22 calyx of Held nerve terminals. ns, nonsignificant, $^*p < 0.05$.

mate release with TEA did not increase the CP-AMPAR percentage block.

We next investigated whether TEA-induced spike broadening, which potentiates presynaptic glutamate release and activates more postsynaptic AMPARs, would lead to detectable Ca^{2+} transients in the principal cells of the MNTB. We included OGB-1 in the recording pipette and performed whole-cell recordings on principal cells in the P18–P22 group in an effort to detect CP-AMPAR-mediated Ca^{2+} transients in the continued presence of TEA. Even with TEA, afferent fiber stimulation only produced a 2.6 ± 1.3% increase in fluorescence in the postsynaptic compartment and application of IEM-1460 did not change this response (IEM-1460: 2.7 ± 1.1% increase in fluorescence; Fig. 7*D1–D3*). To further investigate this, we used P27–P30 animals, excluded EGTA completely from the OGB-1-loading pipette, and increased the 100 Hz afferent fiber stimulation duration to 1 s. Under these conditions, we detected a 4.5 ± 0.7% increase in fluorescence in the principal cells of the MNTB in response to synaptic stimulation. Application of IEM-1460 to the slices blocked 33.4 ± 17.3% of this response, resulting in a 2.6 ± 0.4% increase in fluorescence (Fig. 8*A1–A3*). These data confirm that functional CP-AMPARs are present at the more mature P27–P30 principal cells of the MNTB, but in reduced numbers.

CP-AMPAR regulation of postsynaptic spiking fidelity

We next sought to test the functional contribution of CP-AMPARs to postsynaptic spiking. We recorded HFS AP trains in current-clamp mode for control conditions or after the addition of IEM-1460 (Fig. 9*A*). These experiments were performed at PT (33–35°C) to elicit HFS (100 Hz) without failures. They were also done in the continued presence of DL-AP5 (50 μM) to inhibit NMDA receptors (Taschenberger and von Gersdorff, 2000; Futai et al., 2001). Moreover, the principal cells were current injected to a resting membrane potential of ~−70 mV throughout the entirety of the recording (Fig. 9*B*). We found that inhibiting CP-AMPARs produced a significant increase in the frequency of AP failures in the P8–P11 group (control: 0.2 ± 0.2%; IEM-1460: 35.5 ± 13.6%), whereas no effect was observed in the P18–P22 group (control: 2.3 ± 1.4%, IEM-1460: 4.1 ± 2.2%; Fig. 9*C*). We additionally analyzed several parameters of the first AP of the train (Fig. 9*D*). We found that IEM-1460 inhibited the peak amplitude of the postsynaptic MNTB principal cell AP at both age ranges, albeit more strongly in the P8–P11 group (Fig. 9*E*). In addition, IEM-1460 reduced the depolarizing afterpotential significantly for the P8–P11 group (Fig. 9*D*), which is probably due to the slow decay of EPSCs (Fig. 1*C*; Johnston et al., 2009) and the slow discharge of the unmyelinated axon capacitance (Borst et al., 1995; Kim et al., 2010). The AP half-width remained unaffected in both age groups, whereas the AP peak delay was increased in

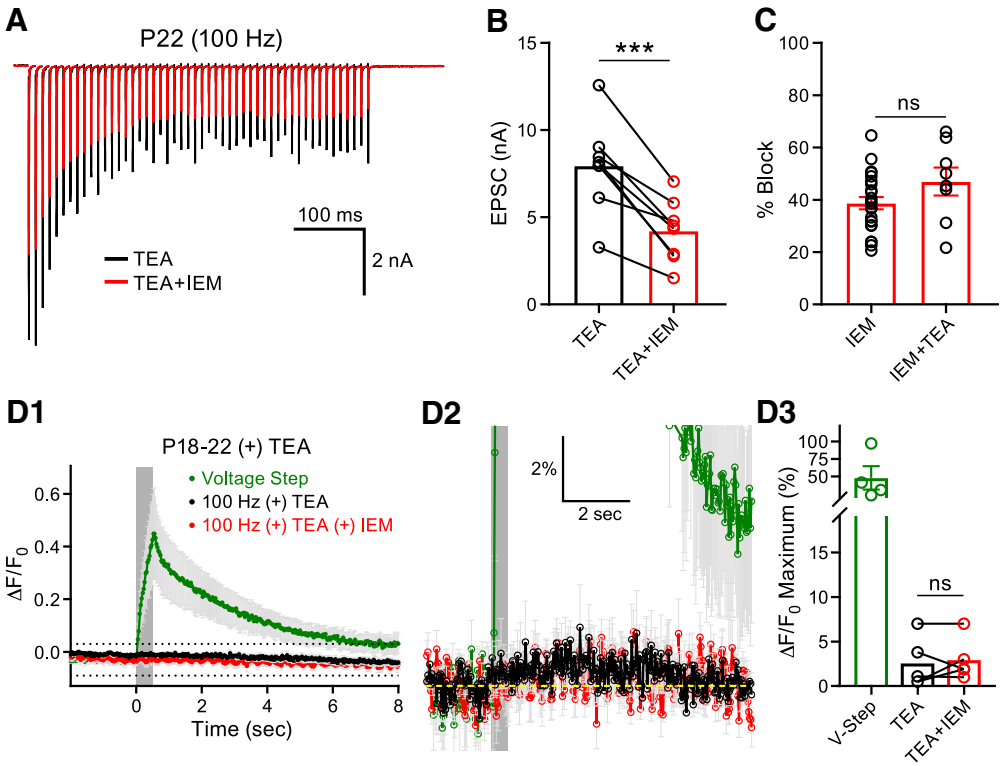

Figure 7. CP-AMPAR-mediated Ca^{2+} transients are undetectable in mature principal cells recorded in the presence of TEA. ***A***, Midline stimulation was used to evoke EPSCs at 100 Hz for 500 ms in the presence of TEA (black) or in TEA + IEM-1460 (red). ***B***, Addition of IEM-1460 reduced the first EPSC peak amplitude (paired *t* test: $n = 8, p = 0.0004$). ***C***, In the P18–P22 group, the percentage block induced by the addition of IEM-1460 alone (Figs. 1*D*, 3*F*) was compared with that recorded in the presence IEM-1460 + TEA. No difference was detected (unpaired *t* test; IEM-1460: $n = 23$; IEM-1460 + TEA: $n = 8$, $p = 0.1141$). ***D1***, OGB1 was used to simultaneously record Ca^{2+} transients from the principal cells of the MNTB induced by midline stimulation (gray box denotes stimulation) at a holding potential of −70 mV. The average responses are presented in the presence of TEA (black) and TEA + IEM (red). The Ca^{2+} response induced by a postsynaptic depolarization in TEA (green) is shown for comparison. ***D2***, Region outlined by dotted lines in ***D1*** at higher magnification. Ca^{2+} transients evoked by midline stimulation were unchanged in the presence of TEA and TEA + IEM. ***D3***, Summary data of the peak Ca^{2+} responses in the P18–P22 group recorded in the presence of TEA and TEA + IEM (paired *t* test; $n = 5, p = 0.6370$). ns, nonsignificant, $^{***}p < 0.001$.

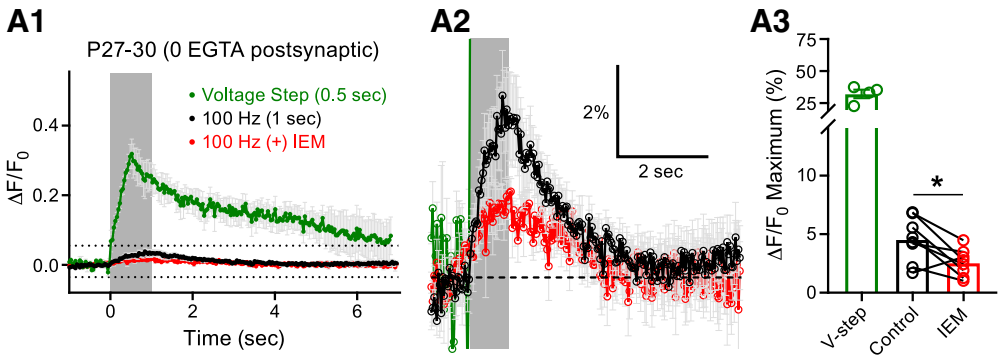

Figure 8. Increasing synaptic drive and limiting EGTA in the loading pipette unveils CP-AMPAR-mediated Ca^{2+} transients in mature principal cells. ***A1***, OGB1 was used to record Ca^{2+} transients from the principal cells of the MNTB induced by midline stimulation at a frequency of 100 Hz from P27–P30 mice. EGTA was excluded from the loading pipette and the stimulation time was increased to 1 s. Midline stimulation (gray box denotes stimulation) produced a Ca^{2+} response (control, black) and application of IEM-1460 inhibited this response (IEM, red). The Ca^{2+} response to a 500 ms postsynaptic voltage-clamp step depolarization is shown for comparison (green). ***A2***, Region outlined by dotted lines in ***A1*** shown at higher magnification. ***A3***, Summary data of the peak Ca^{2+} responses recorded in the P27–P30 group in control conditions or after the addition of IEM-1460 (paired *t* test; $n = 8, p = 0.0170$). ns, nonsignificant, $^{*}p < 0.05$.

both ages (Fig. 9*F*,*G*). These data support the notion that CP-AMPARs play a major role in triggering the postsynaptic AP before the onset of hearing given that application of IEM-1460 had a profound effect on the rate of AP failures. However, the CP-AMPARs appear to play a very minor role in spike timing and no role in failures during 100 Hz stimulation at more mature P18–P22 calyx of Held synapses.

Discussion

We have shown that IEM-1460 blocks ~80% of the EPSC amplitude in immature P4–P5 calyx synapses. CP-AMPARs thus play a major role during the period right after the single, large calyx synapse is established and strengthened on the principal cell soma (Hoffpauir et al., 2009). The expression of CP-AMPARs is then progressively downregulated. Our data show that 1 Hz stimula-

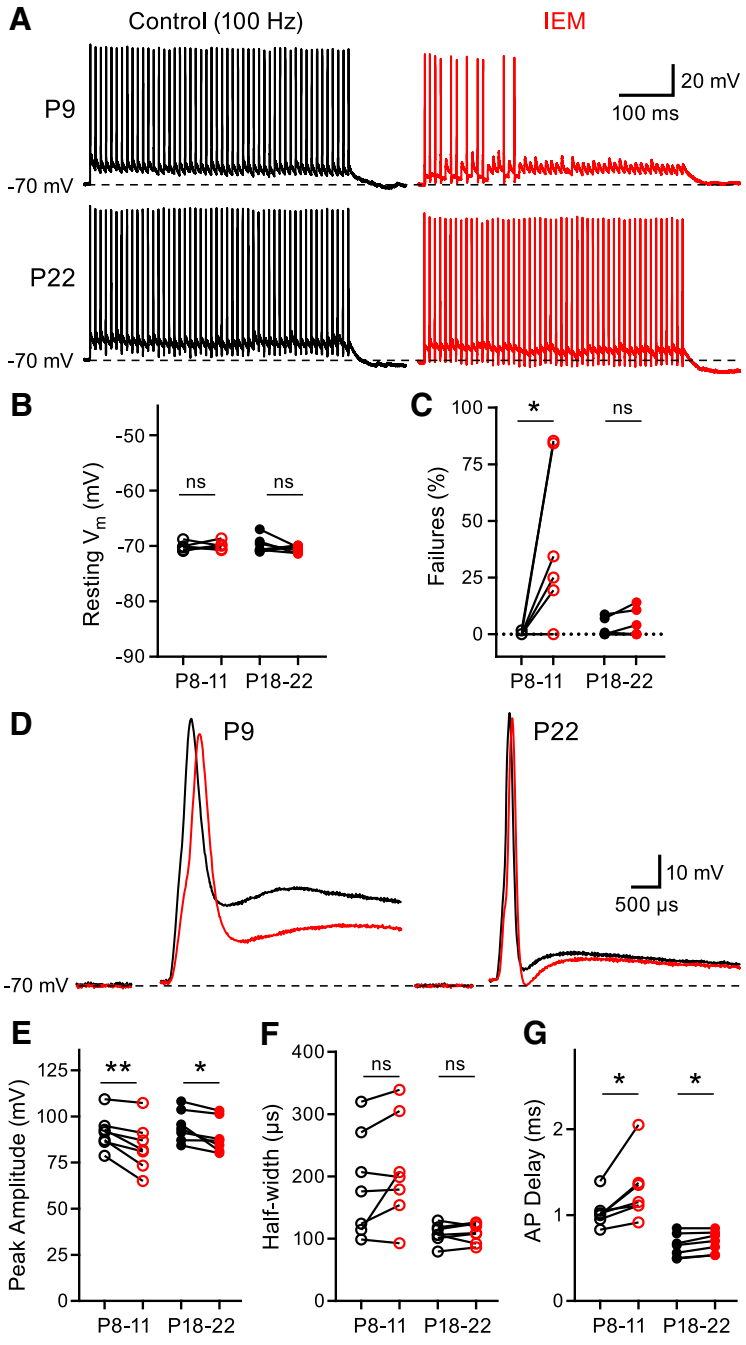

Figure 9. Inhibiting CP-AMPARs impairs synaptic fidelity in juvenile principal cells, but not in mature principal cells. ***A***, Representative AP trains elicited by 500 ms midline stimulation at 100 Hz recorded from a P9 animal (top) and a P22 animal (bottom) in control conditions (black) or after the addition of IEM-1460 (red). All recordings were performed at a PT of 33–35°C and DL-AP5 (50 μM) was included in the extracellular solution to inhibit NMDA receptors. ***B***, Cells were current injected to normalize resting membrane potential to ~−70 mV (paired *t* test; P8–P11: $n = 7$, $p = 0.7152$; P18–P22: $n = 7$, $p = 0.3451$). ***C***, IEM-1460 increases AP failures in the P8–P11 group, but not in the P18–P22 group (paired *t* test; P8–P11: $n = 7$, $p = 0.0396$; P18–P22: $n = 7$, $p = 0.1494$). ***D–G***, First AP from the representative traces shown in ***A*** used to compare several parameters (***D***; tested using paired *t* test; P8–P11: $n = 7$; P18–P22: $n = 7$) of the AP waveform such as AP peak amplitude (***E***; P8–P11: $p = 0.0062$; P18–P22: $p = 0.0214$), half-width (***F***; P8–P11: $p = 0.1246$; P18–P22: $p = 0.6696$), and AP delay (***G***; P8–P11: $p = 0.0184$; P18–P22: $p = 0.0136$). ns, nonsignificant, $^*p < 0.05$, $^{**}p < 0.005$.

tion produces a progressive, activity-dependent block of the EPSCs by IEM-1460, consistent with recent cryo-EM mechanistic studies of open channel block of CP-AMPARs by adamantane derivatives and spider toxins (Twomey et al., 2018). Importantly, the EPSC amplitude measurements were taken after only 40 s of continuous 1 Hz stimulation. The contributions of AMPAR desensitization to short-term synaptic depression are minimal using this low-frequency 1 Hz stimulation (Wong et al., 2003; Renden et al., 2005). Additionally, we were able to obtain a complete recovery from the effect of IEM-1460, which suggests that our results are not influenced by synaptic rundown. The reduction in the EPSC at P18–P22 (40.8 ± 2.7%) is close to that reported previously in P14 mice (43%) using a different CP-AMPAR antagonist (Joshi et al., 2004). We confirmed that the blocking efficiency of IEM-1460 was maximal with continuous 1 Hz stimulation because increasing the stimulation frequency to 100 Hz did not further inhibit the amplitude of the EPSCs.

Spontaneous mEPSCs and AP-evoked EPSCs

We found that mEPSCs and EPSCs evoked by afferent fiber stimulation were comparably inhibited by IEM-1460. Because the EPSCs were reduced by 68% and 41% at P8–P11 and P18–P22, respectively, we predicted that the average amplitude of the mEPSCs in IEM-1460 would be ~22 pA at P8–P11 and 44 pA at P18–P22 based on our control mEPSC measurements. Accordingly, when we performed Gaussian function fits on our peak amplitude distributions and constrained the mean of the fits to the aforementioned predicted values, we obtained curves that closely approximated the peak amplitude distributions. Because our curve fit predictions closely matched our mEPSC amplitude distributions, these data suggest that the AMPARs mediating mEPSCs and evoked EPSCs are indistinguishable from one another with respect to AMPAR subunit composition (Kavalali, 2015; Tsintsadze et al., 2017).

Postsynaptic Ca^{2+} imaging during development

To record Ca^{2+} transients, the MNTB principal cells were continuously held at −70 mV, thereby limiting the contributions of NMDA and voltage-gated Ca^{2+} channels to the Ca^{2+} influx (Bollmann et al., 1998). Additionally, maintaining the cell at a holding potential of −70 mV produced a constant and high driving force for Ca^{2+} ion passage through open CP-AMPARs. We excluded polyamines from the recording pipette in an effort to limit their possible antagonistic effects on CP-AMPARs (Bowie and Mayer, 1995). We were surprised to observe significant CP-AMPAR-mediated responses in the P8–P11 group because AMPAR desensitization to 100 Hz stimulation is quite robust at this age (Renden et al., 2005). Desensitization may indeed limit Ca^{2+} flux by CP-AMPARs. How-

ever, we opted not to use cyclothiazide (CTZ) to block desensitization because of its effects on presynaptic P_r (Ishikawa and Takahashi, 2001), although the inclusion of CTZ does produce stronger cobalt uptake via CP-AMPARs (Eybalin et al., 2004).

Using confocal laser imaging, we were unable to detect an effect of IEM-1460 on the CP-AMPAR-mediated Ca^{2+} transients in the P18–P22 group in both the absence and presence of TEA, although we predicted from our EPSC recordings that likely 30–40% of the AMPARs are permeable to Ca^{2+}. However, upon removal of 0.5 mM EGTA from the patch pipette and increasing the stimulation time to 1 s at a frequency of 100 Hz, we were able to observe a clear effect of IEM-1460 on the Ca^{2+} transients. These Ca^{2+} transients may be difficult to observe in the mature MNTB principal cells because the postsynaptic AMPARs preferentially cluster in progressively smaller areas during development (Hermida et al., 2010). Therefore, the Ca^{2+} flux may only exist in small microdomains under the synaptic cleft. Additionally, Ca^{2+} buffering becomes stronger and faster in the principal cell with age because several different types of Ca^{2+} binding proteins are upregulated with development (Lohmann and Friauf, 1996; Felmy and Schneggenburger, 2004).

Synaptic AMPAR subunits change during development

The temporal expression patterns of GluA2 in the MNTB, the critical regulator of Ca^{2+} permeability, are not in complete agreement in the literature. Developmental studies of MNTB suggested that GluA2 levels are quite high throughout the first two postnatal weeks and decline rapidly during the third postnatal week (Caicedo and Eybalin, 1999). However, a subsequent study suggests GluA2 is low during early postnatal development and is likely not necessary for MNTB synaptogenesis (Joshi et al., 2004). Our results in P4–P5 synapses agree with this particular finding. Conversely, measurements of the mRNA levels coding for the GluA2 subunit suggest that GluA2 is actually the second most abundant subunit and that these mRNA levels remain stable throughout development (Koike-Tani et al., 2005).

The GluA4 subunit is indispensable for the high-fidelity transmission of the calyx of Held synapse (Joshi et al., 2004; Yang et al., 2011). However, our results are in contrast to those of Joshi et al. (2004) suggesting high Ca^{2+} permeability through the AMPARs after hearing onset. Their conclusion is supported by rectifying *I–V* relationships at P13–P14 and by the lack of immunohistochemical staining for GluA2 upon maturation. Although the rectification index is generally agreed upon to be a measure of AMPAR subunit composition, the sensitivity as a readout for Ca^{2+} permeability remains controversial. In hippocampal interneurons, the amount of GluA2 necessary to abolish IV rectification in AMPARs is higher than that needed to abolish Ca^{2+} permeability (Washburn et al., 1997). Accordingly, 50% of the interneurons that possessed rectifying *I–V*s were also positive for GluA2 (Washburn et al., 1997). Conversely, in retinal bipolar cells of salamander and auditory cochlear nucleus chick neurons, the EPSC *I–V* curves were linear while retaining high divalent ion permeability (Gilbertson et al., 1991; Otis et al., 1995), although in these experiments, the investigators did not add polyamines to the patch pipette. Therefore, using the rectification index obtained from *I–V* plots of EPSCs may not be an accurate readout for the Ca^{2+} permeability of AMPARs in all scenarios because the structural components that mediate Ca^{2+} permeability and polyamine block are different.

Diversity of AMPARs and release probability at auditory brainstem nuclei

CP-AMPARs are found in a subclass interneurons in the neocortex, where they regulate the dynamic balance of excitation and inhibition (Hull et al., 2009; Lalanne et al., 2016). At the inner hair cell synapse of the cochlea, a ribbon-type synapse, CP-AMPARs are expressed at the afferent fibers before the onset of hearing and their expression declines with maturation (Eybalin et al., 2004; Reijntjes and Pyott, 2016), although some receptors may remain in mature fibers (Sebe et al., 2017). Likewise, in the superior paraolivary nucleus of mice, a mixed population of CP-AMPARs and Ca^{2+}-impermeable AMPARs were present before hearing onset; however, upon maturation, the population was composed primarily of Ca^{2+}-impermeable AMPARs (Felix and Magnusson, 2016). However, in the same study, it was concluded that neurons of the lateral superior olive retain a mixed population of CP-AMPARs and Ca^{2+}-impermeable AMPARs throughout development (Felix and Magnusson, 2016). Indeed, many regions in the auditory brainstem have high expression of CP-AMPARs (Otis et al., 1995; Ravindranathan et al., 2000; Gardner et al., 2001; Takago and Oshima-Takago, 2018).

Several factors can modulate the Ca^{2+} permeability of the AMPAR past the level of GluA2 subunit inclusion. For example, the functional consequence of auxiliary proteins on the biophysical properties of AMPARs have been discovered only recently (Bowie, 2018). In addition to the regulation of AMPAR trafficking, these proteins can bidirectionally modulate single-channel unitary conductance, Ca^{2+} permeability, and EPSC rectification (Wollmuth, 2018). The auxiliary subunits stargazin and cornichon can increase Ca^{2+} permeability (Kott et al., 2009; Coombs et al., 2012), whereas the recently discovered auxiliary subunit GSG1L reduces Ca^{2+} permeability (McGee et al., 2015). The developmental expression profile of the AMPAR auxiliary subunits in the auditory brainstem remains unknown and awaits future studies.

Our results suggest that P4–P5 synapses have a high P_r and low abundance of synaptic GluA2, making them highly Ca^{2+} permeable, whereas adult-like P30–P34 synapses are more diverse and have on average lower P_r. We propose that mature synapses express both GluA2 and GluA4 subunits, making their AMPARs fast and impermeable to Ca^{2+}. Changes in spontaneous and patterned spike activity during postnatal development may propel higher expression levels of GluA2 and lower P_r values (Tokuoka and Goda, 2008; Babola et al., 2018), whereas sound-driven spiking activity may subsequently stabilize GluA2 expression and short-term plasticity (Hermann et al., 2007; Ngodup et al., 2015). Loss of CP-AMPARs seems to coincide with the downregulation of NMDARs over the critical developmental window of hearing onset (Taschenberger and von Gersdorff, 2000; Futai et al., 2001). It appears that limiting postsynaptic Ca^{2+} flux is important for high-fidelity transmission at this synapse. A sparse expression of CP-AMPARs and NMDARs at mature synapses may also reduce the likelihood of excitotoxicity associated with Ca^{2+} influx. An AMPAR subunit combination with a predominant ratio of GluA2:GluA4 near 1:3 thus represents an attractive possible scenario: Ca^{2+} permeability is blocked, whereas fast gating kinetics, high unitary conductance, and faster recovery from desensitization are maintained.

References

Babola TA, Li S, Gribizis A, Lee BJ, Issa JB, Wang HC, Crair MC, Bergles DE (2018) Homeostatic control of spontaneous activity in the developing auditory system. Neuron 99:511–524.

Bollmann JH, Helmchen F, Borst JG, Sakmann B (1998) Postsynaptic Ca^{2+} influx mediated by three different pathways during synaptic transmission at a calyx-type synapse. J Neurosci 18:10409–10419.

Borst JG, Helmchen F, Sakmann B (1995) Pre- and postsynaptic whole-cell recordings in the medial nucleus of the trapezoid body of the rat. J Physiol 489:825–840.

Bowie D (2018) Polyamine-mediated channel block of ionotropic glutamate receptors and its regulation by auxiliary proteins. J Biol Chem 293:18789–18802.

Bowie D, Mayer ML (1995) Inward rectification of both AMPA and kainate subtype glutamate receptors generated by polyamine-mediated ion channel block. Neuron 15:453–462.

Brusa R, Zimmermann F, Koh DS, Feldmeyer D, Gass P, Seeburg PH, Sprengel R (1995) Early-onset epilepsy and postnatal lethality associated with an editing-deficient GluR-B allele in mice. Science 270:1677–1680.

Burnashev N, Monyer H, Seeburg PH, Sakmann B (1992) Divalent ion permeability of AMPA receptor channels is dominated by the edited form of a single subunit. Neuron 8:189–198.

Caicedo A, Eybalin M (1999) Glutamate receptor phenotypes in the auditory brainstem and mid-brain of the developing rat. Eur J Neurosci 11:51–74.

Carlson NG, Howard J, Gahring LC, Rogers SW (2000) RNA editing (Q/R site) and flop/flip splicing of AMPA receptor transcripts in young and old brains. Neurobiol Aging 21:599–606.

Carriedo SG, Yin HZ, Sensi SL, Weiss JH (1998) Rapid Ca^{2+} entry through Ca^{2+}-permeable AMPA/Kainate channels triggers marked intracellular Ca^{2+} rises and consequent oxygen radical production. J Neurosci 18: 7727–7738.

Chen Z, Das B, Nakamura Y, DiGregorio DA, Young SM Jr (2015) Ca^{2+} channel to synaptic vesicle distance accounts for the readily releasable pool kinetics at a functionally mature auditory synapse. J Neurosci 35: 2083–2100.

Coombs ID, Soto D, Zonouzi M, Renzi M, Shelley C, Farrant M, Cull-Candy SG (2012) Cornichons modify channel properties of recombinant and glial AMPA receptors. J Neurosci 32:9796–9804.

Dingledine R, Borges K, Bowie D, Traynelis SF (1999) The glutamate receptor ion channels. Pharmacol Rev 51:7–61.

Elmqvist D, Quastel DM (1965) A quantitative study of end-plate potentials in isolated human muscle. J Physiol 178:505–529.

Eybalin M, Caicedo A, Renard N, Ruel J, Puel JL (2004) Transient Ca^{2+}-permeable AMPA receptors in postnatal rat primary auditory neurons. Eur J Neurosci 20:2981–2989.

Felix RA 2nd, Magnusson AK (2016) Development of excitatory synaptic transmission to the superior paraolivary and lateral superior olivary nuclei optimizes differential decoding strategies. Neuroscience 334:1–12.

Felmy F, Schneggenburger R (2004) Developmental expression of the Ca^{2+}-binding proteins calretinin and parvalbumin at the calyx of held of rats and mice. Eur J Neurosci 20:1473–1482.

Ford MC, Grothe B, Klug A (2009) Fenestration of the calyx of held occurs sequentially along the tonotopic axis, is influenced by afferent activity, and facilitates glutamate clearance. J Comp Neurol 514:92–106.

Forsythe ID, Barnes-Davies M (1993) The binaural auditory pathway: excitatory amino acid receptors mediate dual timecourse excitatory postsynaptic currents in the rat medial nucleus of the trapezoid body. Proc Biol Sci 251:151–157.

Futai K, Okada M, Matsuyama K, Takahashi T (2001) High-fidelity transmission acquired via a developmental decrease in NMDA receptor expression at an auditory synapse. J Neurosci 21:3342–3349.

Gardner SM, Trussell LO, Oertel D (2001) Correlation of AMPA receptor subunit composition with synaptic input in the mammalian cochlear nuclei. J Neurosci 21:7428–7437.

Gilbertson TA, Scobey R, Wilson M (1991) Permeation of calcium ions through non-NMDA glutamate channels in retinal bipolar cells. Science 251:1613–1615.

González-Inchauspe C, Urbano FJ, Di Guilmi MN, Uchitel OD (2017) Acid-sensing ion channels activated by evoked released protons modulate synaptic transmission at the mouse calyx of held synapse. J Neurosci 37:2589–2599.

Grande G, Wang LY (2011) Morphological and functional continuum underlying heterogeneity in the spiking fidelity at the calyx of held synapse in vitro. J Neurosci 31:13386–13399.

Hermann J, Pecka M, von Gersdorff H, Grothe B, Klug A (2007) Synaptic transmission at the calyx of held under *in vivo*-like stimulation patterns. J Neurophysiol 98:807–820.

Hermida D, Mateos JM, Elezgarai I, Puente N, Bilbao A, Bueno-López JL, Streit P, Grandes P (2010) Spatial compartmentalization of AMPA glutamate receptor subunits at the calyx of held synapse. J Comp Neurol 518:163–174.

Hoffpauir BK, Marrs GS, Mathers PH, Spirou GA (2009) Does the brain connect before the periphery can direct? A comparison of three sensory systems in mice. Brain Res 1277:115–129.

Hollmann M, Hartley M, Heinemann S (1991) Ca^{2+} permeability of KA-AMPA-gated glutamate receptor channels depends on subunit composition. Science 252:851–853.

Hull C, Isaacson JS, Scanziani M (2009) Postsynaptic mechanisms govern the differential excitation of cortical neurons by thalamic inputs. J Neurosci 29:9127–9136.

Hume RI, Dingledine R, Heinemann SF (1991) Identification of a site in glutamate receptor subunits that controls calcium permeability. Science 253:1028–1031.

Ishikawa T, Takahashi T (2001) Mechanisms underlying presynaptic facilitatory effect of cyclothiazide at the calyx of held of juvenile rats. J Physiol 533:423–431.

Iwasaki S, Takahashi T (2001) Developmental regulation of transmitter release at the calyx of held in rat auditory brainstem. J Physiol 534:861–871.

Jia Z, Agopyan N, Miu P, Xiong Z, Henderson J, Gerlai R, Taverna FA, Velumian A, MacDonald J, Carlen P, Abramow-Newerly W, Roder J (1996) Enhanced LTP in mice deficient in the AMPA receptor GluR2. Neuron 17:945–956.

Johnston J, Postlethwaite M, Forsythe ID (2009) The impact of synaptic conductance on action potential waveform: evoking realistic action potentials with a simulated synaptic conductance. J Neurosci Methods 183: 158–164.

Johnston J, Forsythe ID, Kopp-Scheinpflug C (2010) Going native: voltage-gated potassium channels controlling neuronal excitability. J Physiol 588: 3187–3200.

Joshi I, Shokralla S, Titis P, Wang LY (2004) The role of AMPA receptor gating in the development of high-fidelity neurotransmission at the calyx of held synapse. J Neurosci 24:183–196.

Kandler K, Friauf E (1993) Pre- and postnatal development of efferent connections of the cochlear nucleus in the rat. J Comp Neurol 328:161–184.

Kavalali ET (2015) The mechanisms and functions of spontaneous neurotransmitter release. Nat Rev Neurosci 16:5–16.

Kim JH, Kushmerick C, von Gersdorff H (2010) Presynaptic resurgent Na^+ currents sculpt the action potential waveform and increase the firing reliability at a CNS nerve terminal. J Neurosci 30:15479–15490.

Kim MH, von Gersdorff H (2016) Postsynaptic plasticity triggered by Ca^{2+}-permeable AMPA receptor activation in retinal amacrine cells. Neuron 89:507–520.

Koike-Tani M, Saitoh N, Takahashi T (2005) Mechanisms underlying developmental speeding in AMPA-EPSC decay time at the calyx of held. J Neurosci 25:199–207.

Kopp-Scheinpflug C, Steinert JR, Forsythe ID (2011) Modulation and control of synaptic transmission across the MNTB. Hear Res 279:22–31.

Kott S, Sager C, Tapken D, Werner M, Hollmann M (2009) Comparative analysis of the pharmacology of GluR1 in complex with transmembrane AMPA receptor regulatory proteins gamma2, gamma3, gamma4, and gamma8. Neuroscience 158:78–88.

Krächan EG, Fischer AU, Franke J, Friauf E (2017) Synaptic reliability and temporal precision are achieved via high quantal content and effective replenishment: auditory brainstem versus hippocampus. J Physiol 595: 839–864.

Kuner T, Beck C, Sakmann B, Seeburg PH (2001) Channel-lining residues of the AMPA receptor M2 segment: structural environment of the Q/R site and identification of the selectivity filter. J Neurosci 21:4162–4172.

Lalanne T, Oyrer J, Mancino A, Gregor E, Chung A, Huynh L, Burwell S, Maheux J, Farrant M, Sjöström PJ (2016) Synapse-specific expression of calcium-permeable AMPA receptors in the neocortical layer 5. J Physiol 594:837–861.

Lohmann C, Friauf E (1996) Distribution of the calcium-binding proteins parvalbumin and calretinin in the auditory brainstem of adult and developing rats. J Comp Neurol 367:90–109.

Lorteije JA, Rusu SI, Kushmerick C, Borst JG (2009) Reliability and precision of mouse calyx of held synapse. J Neurosci 29:13770–13784.

Lujan B, Kushmerick C, Banerjee TD, Dagda RK, Renden R (2016) Glycolysis selectively shapes the presynaptic action potential waveform. J Neurophysiol 116:2523–2540.

McGee TP, Bats C, Farrant M, Cull-Candy SG (2015) Auxiliary subunit GSG1L acts to suppress calcium-permeable AMPA receptor function. J Neurosci 35:16171–16179.

Neher E (2015) Merits and limitations of vesicle pool models in view of heterogeneous populations of synaptic vesicles. Neuron 87:1131–1142.

Ngodup T, Goetz JA, McGuire BC, Sun W, Lauer AM, Xu-Friedman MA (2015) Activity-dependent, homeostatic regulation of neurotransmitter release from auditory nerve fibers. Proc Natl Acad Sci U S A 112:6479–6484.

Noh KM, Yokota H, Mashiko T, Castillo PE, Zukin RS, Bennett MV (2005) Blockade of calcium-permeable AMPA receptors protects hippocampal neurons against global ischemia-induced death. Proc Natl Acad Sci U S A 102:12230–12235.

Otis TS, Raman IM, Trussell LO (1995) AMPA receptors with high Ca^{2+} permeability mediate synaptic transmission in the avian auditory pathway. J Physiol 482:309–315.

Park P, Sanderson TM, Amici M, Choi SL, Bortolotto ZA, Zhuo M, Kaang BK, Collingridge GL (2016) Calcium-permeable AMPA receptors mediate the induction of the protein kinase A-dependent component of long-term potentiation in the hippocampus. J Neurosci 36:622–631.

Plant K, Pelkey KA, Bortolotto ZA, Morita D, Terashima A, McBain CJ, Collingridge GL, Isaac JT (2006) Transient incorporation of native GluR2-lacking AMPA receptors during hippocampal long-term potentiation. Nat Neurosci 9:602–604.

Portfors CV, von Gersdorff H (2013) Macrocircuits for sound localization use leaky coincidence detectors and specialized synapses. Neuron 78:755–757.

Ravindranathan A, Donevan SD, Sugden SG, Greig A, Rao MS, Parks TN (2000) Contrasting molecular composition and channel properties of AMPA receptors on chick auditory and brainstem motor neurons. J Physiol 523:667–684.

Reijntjes DOJ, Pyott SJ (2016) The afferent signaling complex: regulation of type I spiral ganglion neuron responses in the auditory periphery. Hear Res 336:1–16.

Renden R, Taschenberger H, Puente N, Rusakov DA, Duvoisin R, Wang LY, Lehre KP, von Gersdorff H (2005) Glutamate transporter studies reveal the pruning of metabotropic glutamate receptors and absence of AMPA receptor desensitization at mature calyx of held synapses. J Neurosci 25:8482–8497.

Rosenmund C, Clements JD, Westbrook GL (1993) Nonuniform probability of glutamate release at a hippocampal synapse. Science 262:754–757.

Sebe JY, Cho S, Sheets L, Rutherford MA, von Gersdorff H, Raible DW (2017) Ca^{2+}-permeable AMPARs mediate glutamatergic transmission and excitotoxic damage at the hair cell ribbon synapse. J Neurosci 37:6162–6175.

Spirou GA, Brownell WE, Zidanic M (1990) Recordings from cat trapezoid body and HRP labeling of globular bushy cell axons. J Neurophysiol 63:1169–1190.

Spirou GA, Chirila FV, von Gersdorff H, Manis PB (2008) Heterogeneous Ca^{2+} influx along the adult calyx of held: structural and computational study. Neuroscience 154:171–185.

Takago H, Oshima-Takago T (2018) Pre- and postsynaptic ionotropic glutamate receptors in the auditory system of mammals. Hear Res 362:1–13.

Taschenberger H, von Gersdorff H (2000) Fine-tuning an auditory synapse for speed and fidelity: developmental changes in presynaptic waveform, EPSC kinetics, and synaptic plasticity. J Neurosci 20:9162–9173.

Taschenberger H, Leão RM, Rowland KC, Spirou GA, von Gersdorff H (2002) Optimizing synaptic architecture and efficiency for high-frequency transmission. Neuron 36:1127–1143.

Taschenberger H, Woehler A, Neher E (2016) Superpriming of synaptic vesicles as a common basis for intersynapse variability and modulation of synaptic strength. Proc Natl Acad Sci U S A 113:E4548–E4557.

Tokuoka H, Goda Y (2008) Activity-dependent coordination of presynaptic release probability and postsynaptic GluR2 abundance at single synapses. Proc Natl Acad Sci U S A 105:14656–14661.

Traynelis SF, Wollmuth LP, McBain CJ, Menniti FS, Vance KM, Ogden KK, Hansen KB, Yuan H, Myers SJ, Dingledine R (2010) Glutamate receptor ion channels: structure, regulation, and function. Pharmacol Rev 62:405–496.

Tsintsadze T, Williams CL, Weingarten DJ, von Gersdorff H, Smith SM (2017) Distinct actions of voltage-activated Ca^{2+} channel block on spontaneous release at excitatory and inhibitory central synapses. J Neurosci 37:4301–4310.

Twomey EC, Yelshanskaya MV, Vassilevski AA, Sobolevsky AI (2018) Mechanisms of channel block in calcium-permeable AMPA receptors. Neuron 99:956–968.

von Gersdorff H, Borst JG (2002) Short-term plasticity at the calyx of held. Nat Rev Neurosci 3:53–64.

Waldmann R, Champigny G, Bassilana F, Heurteaux C, Lazdunski M (1997) A proton-gated cation channel involved in acid-sensing. Nature 386:173–177.

Wang LY, Kaczmarek LK (1998) High-frequency firing helps replenish the readily releasable pool of synaptic vesicles. Nature 394:384–388.

Washburn MS, Numberger M, Zhang S, Dingledine R (1997) Differential dependence on GluR2 expression of three characteristic features of AMPA receptors. J Neurosci 17:9393–9406.

Weiss JH (2011) Ca^{2+} permeable AMPA channels in diseases of the nervous system. Front Mol Neurosci 4:42.

Wollmuth LP (2018) Ion permeation in ionotropic glutamate receptors: still dynamic after all these years. Curr Opin Physiol 2:36–41.

Wong AY, Graham BP, Billups B, Forsythe ID (2003) Distinguishing between presynaptic and postsynaptic mechanisms of short-term depression during action potential trains. J Neurosci 23:4868–4877.

Yang YM, Aitoubah J, Lauer AM, Nuriya M, Takamiya K, Jia Z, May BJ, Huganir RL, Wang LY (2011) GluA4 is indispensable for driving fast neurotransmission across a high-fidelity central synapse. J Physiol 589:4209–4227.